Check for updates

JGR Oceans

RESEARCH ARTICLE
10.1029/2024JC021241

Competition Between Advected and Local Variability Determines Coherent Propagation of Labrador Sea Water Along the DWBC

Anne-Sophie Fortin[1] **and M. Susan Lozier**[1]

[1]School of Earth & Atmospheric Science, Georgia Institute of Technology, Atlanta, GA, USA

Key Points:

- Coherent property propagation along the Deep Western Boundary Current is inferred from lagged correlations
- Labrador Sea Water (LSW) has a distinct behavior as a function of density: We find coherent property propagation only for deep LSW
- Upper LSW local variance exceeds source variance, thereby preventing its coherent propagation by compromising its anomaly signal

Supporting Information:

Supporting Information may be found in the online version of this article.

Correspondence to:

A.-S. Fortin,
afortin3@gatech.edu

Citation:

Fortin, A.-S., & Lozier, M. S. (2024). Competition between advected and local variability determines coherent propagation of Labrador Sea Water along the DWBC. *Journal of Geophysical Research: Oceans*, *129*, e2024JC021241. https://doi.org/10.1029/2024JC021241

Received 17 APR 2024
Accepted 20 NOV 2024

Author Contributions:

Conceptualization: M. Susan Lozier
Data curation: Anne-Sophie Fortin
Formal analysis: Anne-Sophie Fortin
Funding acquisition: M. Susan Lozier
Investigation: Anne-Sophie Fortin, M. Susan Lozier
Methodology: Anne-Sophie Fortin
Project administration: M. Susan Lozier
Resources: Anne-Sophie Fortin
Software: Anne-Sophie Fortin
Supervision: M. Susan Lozier
Validation: Anne-Sophie Fortin
Visualization: Anne-Sophie Fortin
Writing – original draft: Anne-Sophie Fortin
Writing – review & editing: Anne-Sophie Fortin, M. Susan Lozier

© 2024 The Author(s).
This is an open access article under the terms of the Creative Commons Attribution-NonCommercial License, which permits use, distribution and reproduction in any medium, provided the original work is properly cited and is not used for commercial purposes.

Abstract The Deep Western Boundary Current (DWBC) is a major conduit for the equatorward export of dense waters formed in the subpolar North Atlantic and Nordic Seas that constitute the lower limb of the Atlantic Meridional Overturning Circulation. Here, we investigate the extent to which there is coherent propagation of property anomalies along the DWBC from the Labrador Sea exit to 26.5°N. Past studies have focused on relationships between DWBC anomalies at selected sites. Here we use a hydrographic data set (EN4) that covers the time period of 1970–2020 to examine coherence continuously along the boundary current. Our findings reveal sharp differences between the upper and deep Labrador Sea Water (uLSW, dLSW). Specifically, dLSW property anomalies are highly correlated at all points downstream to the Labrador Sea exit. Furthermore, the lags that yield maximum correlations uniformly increase with distance along the boundary. uLSW, however, shows a sharp decline in coherence along the boundary such that the anomalies downstream are poorly correlated with those at the Labrador Sea exit and the lag times are not monotonic. Most of the decline in uLSW coherence occurs from the Labrador Sea exit to Flemish Cap, where local variability at uLSW densities is large. Our study sheds light on the competition between advected property variability and local property variability that impacts the identification of anomalies downstream. The uLSW and dLSW differences expressed along the DWBC are also evident offshore, consistent with past Lagrangian studies.

Plain Language Summary The Deep Western Boundary Current (DWBC) exports dense waters formed in the subpolar North Atlantic and Nordic Seas equatorward and thus plays a key role in the Atlantic Ocean circulation. The properties of these dense water masses at their formation sites vary from year to year. However, how the source variability is expressed downstream is still unclear. Here, we use a hydrographic data set (EN4) to investigate the coherent propagation of source property variability along the DWBC from 1970 to 2020. We focus on the upper and deep Labrador Sea Water (uLSW and dLSW) and find that these water masses have distinct behaviors. Interestingly, we find a notable increase in the local variability for uLSW around the Flemish Cap, that we do not find for dLSW. With a higher variability downstream of the formation region, uLSW anomalies are susceptible to dilution via mixing. Indeed, we find dLSW to have coherent property propagation at all points along the DWBC, from the Labrador Sea exit (53°N) to Abaco (26.5°N), while uLSW correlations with Labrador Sea properties declines sharply after the Flemish Cap (47°N), suggesting that its source anomalies are not preserved downstream of that feature.

1. Introduction

The lower limb of the Atlantic Meridional Overturning Circulation (AMOC) exports cold, fresh, and dense waters formed in the subpolar North Atlantic and Nordic Seas to equatorward latitudes along the Deep Western Boundary Current (DWBC) and interior pathways (Bower et al., 2009, 2011; Lozier et al., 2010, 2022). When these water masses spread from their formation sites, they transport not only signatures of the heat and freshwater acquired at the surface but also signatures of oxygen (Koelling et al., 2022) and anthropogenic carbon dioxide (Brown et al., 2021). As climate change continues apace, the downstream fate of these properties becomes increasingly important to our assessment of the deep ocean as an oxygen and carbon reservoir.

For decades, the DWBC was considered the main conduit for the downstream advection of waters carried in the AMOC lower limb. The advective timescale for this conduit has been estimated by comparing water mass property variability at downstream DWBC locations with the water mass property variability at water mass formation sites. Examples of this linkage are most prevalent for Labrador Sea Water (LSW), an intermediate water mass formed via wintertime convection in the Labrador and Irminger Seas. A host of studies have used in

21699291, 2024, 12, Downloaded from https://agupubs.onlinelibrary.wiley.com/doi/10.1029/2024JC021241 by Georgia Institute Of Technology, Wiley Online Library on [07/01/2025]. See the Terms and Conditions (https://onlinelibrary.wiley.com/terms-and-conditions) on Wiley Online Library for rules of use; OA articles are governed by the applicable Creative Commons License

situ measurements of water properties to estimate the advective time scale for LSW anomalies to reach subtropical latitudes via the DWBC (e.g., Chomiak et al., 2022; Curry et al., 1998; Doney & Jenkins, 1994; Fine et al., 2002; Le Bras et al., 2017; Molinari et al., 1998; Smethie, 1993; Stramma & Rhein, 2001; van Sebille et al., 2011). Interestingly, the estimated time scale differs among these studies even when considering the same pathway, with a transit time for LSW to the subtropics of 10 years in Molinari et al. (1998) and van Sebille et al. (2011); 10–15 years in Doney and Jenkins (1994) and Chomiak et al. (2022); 15 years in Stramma and Rhein (2001); 18 years in Smethie (1993); and 20 years in Fine et al. (2002). In an attempt to reconcile this range of estimates, Le Bras (2023), drawing on the work of Waugh and Hall (2005), notes that transit times estimated from tracers with exponential initial conditions, such as anthropogenic tracers (e.g., Fine et al., 2002; Smethie, 1993), will be slower than those estimated using hydrographic properties (e.g., Chomiak et al., 2022; Molinari et al., 1998). As such, she persuasively argues that there is more agreement than what it may seem without this consideration. Nevertheless, differences persist even when tracking anomalies with the same hydrographic property. Using salinity, Chomiak et al. (2022) estimate an advection time of 3 years for LSW to reach Line W (~38–40°N, 69–70°W) following the strong convection period of 1987–1994 and a time scale of 7 years for the same pathway following the period of weaker convection from 2000 to 2003.

Differences in these downstream advective time scales might be expected given that Lagrangian studies of RAFOS floats and model-simulated trajectories over the past two decades have shown considerable entrainment and detrainment of boundary current waters along the DWBC (Bower et al., 2009, 2011; Lozier et al., 2022). In one observational study, only a small fraction of RAFOS floats (8%) deliberately placed in LSW at 700 and 1,500 m in the DWBC off the Labrador coast remained in the DWBC at the tail of the Grand Banks (Bower et al., 2009). The same study reports entrainment and detrainment along the DWBC in a model-simulated trajectories analysis. Mechanisms reported to be responsible for this entrainment and detrainment include low-frequency variability in the Gulf Stream strength and pathway (Schott et al., 2004, 2006; Spall, 1996a, 1996b); inertial separation of the DWBC due to the bathymetric curvature and steepening of the Flemish Cap (Solodoch et al., 2020); submesoscale coherent vortices (Bower et al., 2013); and instabilities of the DWBC (Solodoch et al., 2016).

In the face of such strong entrainment and detrainment, the surprising issue is not the reported differences in the advective time scale for LSW anomalies, rather that anomalies can be identified at all thousands of kilometers from their formation sites. A recent modeling study (Zou et al., 2019) has shed some light on this issue, primarily by drawing a distinction between the coherent propagation of transport anomalies in the Upper North Atlantic Deep Water (UNADW; a water mass that includes LSW) and that for the Lower North Atlantic Deep Water (LNADW; comprised primarily of the overflow waters from the Arctic that enter the subpolar North Atlantic across the Greenland-Scotland Ridge). This study showed that UNADW anomalies do not propagate coherently to the subtropical gyre despite strong upstream variability. However, the authors found that LNADW transport anomalies do propagate coherently to the subtopics, but only for large anomalies, presumably those large enough to sustain their signature in spite of mixing along the DWBC. While acknowledging that transport anomalies and property anomalies can have different pathways and advective time scales, this study does point to the possibility that the DWBC's efficacy at propagating anomalies is water-mass and/or depth dependent.

Our study seeks to reconcile the expectation of clearly defined advective time scales for the propagation of water mass anomalies from the subpolar to the subtropical gyre along the DWBC with the observed strong entrainment and detrainment along that boundary.

Past observational studies investigating property propagation along the DWBC have mainly relied on hydrographic data at a few sites to infer advective time scales. In addition to this spatial limitation, the length of these observational data sets has been such that they include at most one or two strong events at the upstream convection site. To alleviate these spatial and temporal constraints, we approach our study of DWBC property propagation with the use of the hydrographic data set EN4, which covers the period from 1970 to 2020. With this data set, we assess the propagation of LSW property anomalies continuously along the DWBC from the exit of the Labrador Sea to 26.5°N. Furthermore, while past studies have generally assumed that property variability at DWBC locations is dominated by upstream source water variability rather than local dynamics, we approach our study with the understanding that property variability at any particular DWBC location can be advected into the area and/or generated locally. In fact, it is the competition between these two that forms the basis of our study.

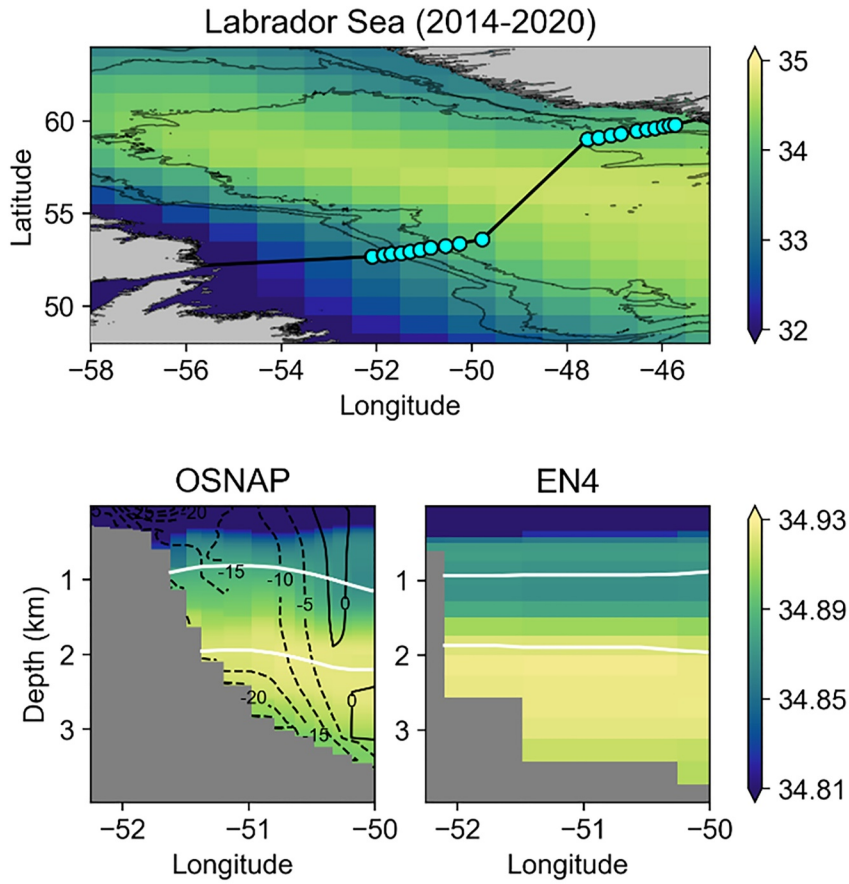

Figure 1. Top panel: Labrador Sea mean surface salinity (2014–2020) from EN4. Overlaid is the OSNAP West section and its mooring positions (bold black line and cyan dots). Bathymetry from General Bathymetric Chart of the Ocean is contoured at 0, 1,000, 2,000, and 3,000 m (thin black lines). Bottom panels: Salinity transect at the Labrador Sea western boundary from OSNAP and EN4 following the nearest OSNAP positions. Also shown are the northward velocities (cm/s) for OSNAP (black contours) and the mean depth of the neutral densities 27.9 (uLSW) and 28.0 (dLSW) for both data sets (white contours). Note that temperature and salinity on the neutral surfaces $\gamma^n = 27.9$ and $\gamma^n = 28.0$ are (3.52°C, 34.88) and (3.15°C, 34.92) for OSNAP and (3.49°C, 34.87) and (3.13°C, 34.92) for EN4, respectively. For reference, the densities $\gamma^n = 27.9$ and $\gamma^n = 28.0$ are equivalent to $\sigma_2 = 36.88$ and $\sigma_2 = 36.97$, respectively, for both OSNAP and EN4.

2. Methods and Data Sets

2.1. Neutral Density Surfaces

To investigate the extent of coherent propagation of property anomalies along the DWBC, we analyze water mass property variability on neutral density surfaces (γ^n; Jackett & McDougall, 1997), which are computed using PreTEOS-10 software. Because of this choice, our analyses of temperature and salinity anomalies yield the same result. Thus, we only present our analysis of the salinity anomalies.

We first select a representative isopycnal for upper and deep LSW (uLSW and dLSW) and then broaden our analysis using a range of isopycnals. For our isopycnal choice, we are guided by Le Bras et al. (2017) who compare water mass definitions in the subpolar North Atlantic and by Chomiak et al. (2023) who use 27.9 and 27.99 to define a shallow and deep LSW convective event. We choose $\gamma^n = 27.9$ and $\gamma^n = 28.0$ as the representative isopycnals for uLSW and dLSW, respectively. These isopycnals reside at an average depth of ~1,000 and 2,000 m, respectively, at the exit of the Labrador Sea (Figure 1). If we compute potential density referenced to 2,000 dbar (σ_2) from temperature and salinity on the 27.9 and 28.0 surfaces at the exit of the Labrador Sea, we obtain 36.88 and 36.97, respectively. In Zou et al. (2019) $\sigma_2 = 36.88$ resides in the UNADW core and $\sigma_2 = 36.97$ resides in the upper range of LNADW. We choose not to investigate water masses with density denser than 28.0 since observations are sparse below 2,000 m (Figure S1 in Supporting Information S1) and we do not have the

21699291, 2024, 12, Downloaded from https://agupubs.onlinelibrary.wiley.com/doi/10.1029/2024JC021241 by Georgia Institute Of Technology, Wiley Online Library on [07/01/2025]. See the Terms and Conditions (https://onlinelibrary.wiley.com/terms-and-conditions) on Wiley Online Library for rules of use; OA articles are governed by the applicable Creative Commons License

confidence that our hydrographic database of choice (EN4, described in the following section) adequately captures temporal variability below that depth. Please see Text S1 and Figures S2–S4 in Supporting Information S1, where we demonstrate that our study conclusions are not impacted by the ocean sampling frequency for $\gamma^n = 27.9$ and $\gamma^n = 28.0$.

2.2. EN4 Objective Analyses

For our analysis we use EN4.2.2, a database of quality-controlled ocean temperature and salinity profiles that draws data from Argo, Arctic Synoptic Basinwide Oceanography, Global Temperature and Salinity Profile Program, and the World Ocean Database 2018 (WOD18). EN4 database extends from 1900 to present, but we consider only the period ranging from 1970 to 2020 in our analysis. Monthly EN4 objective analyses are provided as a gridded data set with 1° horizontal resolution and 42 z-levels with 5 m intervals at the surface increasing in thickness to 300 m at depth. We refer the reader to Good et al. (2013) for detailed EN4 documentation, to Gouretski and Reseghetti (2010) for details about the bias corrections, and to the Met Office Hadley Center observations website to download the EN4 data set.

To allay concerns that our analysis is compromised by the 1° horizontal resolution of EN4, we compare the EN4 salinities with observational data from OSNAP, Line W, and the RAPID array and with the reanalysis product GloSea5. Please see the Supporting Information for this comparison (Text S2 in Supporting Information S1). Overall, there is strong agreement between EN4 and these observations, as evidenced by the comparison of salinity anomalies in Hovmöller diagrams (Figure S5 in Supporting Information S1) and the moderate to strong correlations with salinity observations between neutral density surfaces of 27.9 and 28.0 (Figure S6, Table S1 in Supporting Information S1). Based on these comparisons, we have confidence in EN4's suitability for our analysis.

2.3. GEBCO

The General Bathymetric Chart of the Ocean (GEBCO) data sets provide high-resolution elevation data on a 15 arc-second interval grid (~0.004°) for both land and ocean. We use the GEBCO 2022 data set to define the DWBC pathway in EN4. We first coarsen the GEBCO data set to the EN4 resolution (1°) by averaging GEBCO every 240 grid points of latitude and longitude and then find the position of the 3-km isobath from the exit of the Labrador Sea (52.5°N) to Abaco (26.5°N) that delineates our DWBC pathway. Finally, the properties of EN4 grid points that are nearest to the DWBC pathway are selected. Note that our analysis was repeated for a DWBC pathway following the 2 km isobath contour and those results are consistent with the ones presented here.

3. Results

3.1. Advected Property Variability Along the DWBC

To investigate the propagation of salinity anomalies along the DWBC, we first make a distinction between local variability (Section 3.2) and the variability that is expected due to the advection of property anomalies from an upstream source. We refer to the latter with the simple term "advected variability" and note that it is a component of the total local variability. We create a salinity anomaly time series at each point along the DWBC from the exit of the Labrador Sea to Abaco for the neutral density surfaces 27.9 and 28.0, which represent uLSW and dLSW, respectively. We use these salinity anomaly time series to compute salinity squared correlations with upstream anomaly (R^2) as a function of lag at each point along the DWBC from correlations between local salinity time series and the source time series, that is, at the exit of the Labrador Sea (Figure 2). We highlight any value of R^2 within 0.05 of its maximum at a specific location and define it as our lag range. With this calculation we are determining how much of the local variability can be explained by upstream source variability. The R^2 distribution is then used to determine if there is coherent advection. We characterize the passage of anomalies along the DWBC as "coherent advection" if the following criteria are met: (a) There is at least one statistically significant lagged R^2 value at all points downstream of the source; (b) there is decreasing tendency of the R^2 values in downstream distance; and (c) the advection time, or the lags of the statistically significant R^2 values, increase with distance from the source. We define "patchiness" as the pattern when the above criteria for coherent advection are not met, that is, patchiness is characterized by discontinuities in the R^2 values and/or lag times.

21699291, 2024, 12, Downloaded from https://agupubs.onlinelibrary.wiley.com/doi/10.1029/2024JC021241 by Georgia Institute Of Technology, Wiley Online Library on [07/01/2025]. See the Terms and Conditions (https://onlinelibrary.wiley.com/terms-and-conditions) on Wiley Online Library for rules of use; OA articles are governed by the applicable Creative Commons License

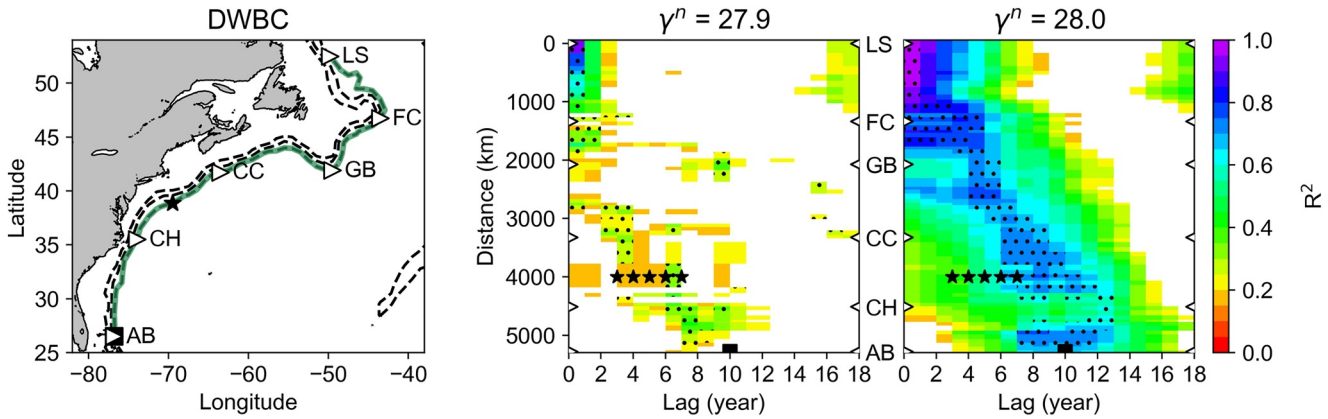

Figure 2. Left panel: Deep Western Boundary Current (DWBC) pathway from the Labrador Sea exit to Abaco, highlighted in green, along the 3,000 m isobath off the American coast. General Bathymetric Chart of the Ocean bathymetry, coarsened to 1° and contoured at 1,000, 2,000, and 3,000 m, is shown as dashed lines. Right panels: Salinity squared correlations with upstream anomaly (R^2) on isopycnals $\gamma^n = 27.9$ (uLSW) and $\gamma^n = 28.0$ (dLSW) along the DWBC pathway as a function of lag and distance from the Labrador Sea exit where the Pearson correlation coefficient (R) is significant with a confidence interval of 99%. Dots indicate where R^2 is within 0.05 of its maximum over lags from 0 to 18 years. Stars indicate a previous estimate of the advective time scale of Labrador Sea Water (LSW) from the central Labrador Sea to Line W for the dLSW mass ($\gamma^n = 27.92$ to 27.98) from Le Bras et al. (2017). Similarly, the square indicates a previous estimate of classical LSW ($\sigma_2 = 36.90$) advection to Abaco from van Sebille et al. (2011). Triangles along the DWBC pathway (left panel) and on the *y*-axis (right panels) indicate the Labrador Sea exit (LS); Flemish Cap (FC); Grand Banks (GB); Cape Cod (CC); Cape Hatteras (CH); and Abaco (AB).

Both uLSW and dLSW anomalies are advected from the exit of the Labrador Sea to the Flemish Cap within 1 year (the max R^2 is found for zero lag). For uLSW, we find a rapid decline in R^2 from the Labrador Sea to the Flemish Cap. Downstream of the Flemish Cap, uLSW max R^2 is low, although mostly statistically significant, and the lag range is patchy, although generally increasing. We acknowledge that local recirculation features could create some ambiguity in the lag structure. For example, the two significant lags at the Grand Banks, that is, 0–2 and 6–10 years, could arise from a recirculation east of the Flemish Cap (Bower et al., 2011). Elsewhere, however, we suggest that the patchiness results from strong mesoscale entrainment and detrainment along the DWBC path that precludes the coherent propagation of uLSW anomalies into the subtropics. Taken together, this indicates strong entrainment and detrainment in the DWBC and rules against the coherent property propagation of uLSW anomalies into the subtropics.

In contrast, dLSW anomalies at all points along the DWBC are well correlated with those at the exit of the Labrador Sea, with a max R^2 ranging from 0.57 to 0.85 downstream of the Flemish Cap. Furthermore, the lag range is continuous and generally increases with distance from Flemish Cap to Cape Hatteras. The lag ranges from 0 to 4 years in the vicinity of Flemish Cap, from 4 to 5 years at the Grand Banks and from 6 to 8 years at Cape Cod. At Line W, the lag range is 6–10 years, which is longer than that estimated by Le Bras et al. (2017), who estimated 3–7 years for dLSW ($\gamma^n = 27.92$ to 27.98) using the Line W data set over the period 2001 to 2014. We elaborate on this difference in Text S3 in Supporting Information S1.

We find a discontinuity in the lag at Cape Hatteras where the local max R^2 is the weakest along the DWBC pathway, and its corresponding lag is 12 years. Further downstream, the max R^2 increases slightly and then at Abaco the lag range is 7–11 years, which is similar to the van Sebille et al. (2011) estimate of 10 years for classical LSW ($\sigma_2 = 36.90$). The discontinuity at Cape Hatteras is consistent with an interior route hypothesized by Bilo and Johns (2019), with detrainment at Cape Hatteras and then re-entrainment at Abaco. This disruption is likely related to the detachment of the Gulf Stream from the coast near Cape Hatteras, entraining dLSW offshore as the Gulf Stream crosses-over the DWBC (Bower & Hunt, 2000). Note that we find similar results if we use the 2,000-m isobath for the DWBC pathway instead of the 3,000-m isobath (Figure S7 in Supporting Information S1).

3.2. Local Property Variability

We now turn our attention to an assessment of local property variability in order to provide context for the results in the previous section. In brief, we compare the local property variability with the advected variability by comparing local salinity variance with the max R^2 along the DWBC. First, we examine the broader spatial field of salinity variance.

21699291, 2024, 12, Downloaded from https://agupubs.onlinelibrary.wiley.com/doi/10.1029/2024JC021241 by Georgia Institute Of Technology, Wiley Online Library on [07/01/2025]. See the Terms and Conditions (https://onlinelibrary.wiley.com/terms-and-conditions) on Wiley Online Library for rules of use; OA articles are governed by the applicable Creative Commons License

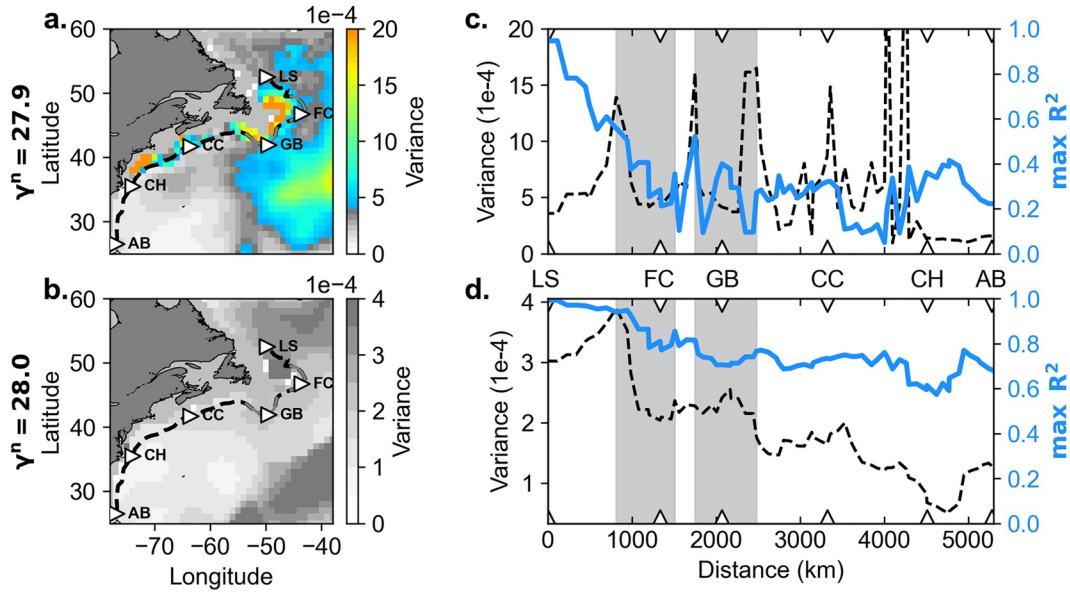

Figure 3. (a, b) Yearly-averaged salinity variance on the (a) 27.9 (uLSW) and (b) 28.0 (dLSW) isopycnal surfaces. The Deep Western Boundary Current (DWBC) pathway from Labrador Sea exit to Abaco is the black dashed line and follows the 3,000 m isobath along the American coast. (c, d) Yearly-averaged salinity variance along the DWBC (dashed black line) and max squared correlations with upstream anomaly (R^2; solid gray line) as a function of distance from the Labrador Sea exit on the neutral isopycnals 27.9 (c) and 28.0 (d). For all panels, triangles indicate the Labrador Sea exit (LS); Flemish Cap (FC); Grand Banks (GB); Cape Cod (CC); Cape Hatteras (CH); and Abaco (AB). The gray lines (a, b) and shadings (c, d) indicate the extent of the FC and GB areas.

On the uLSW isopycnal surface, we find elevated salinity variance ($\sim 5 \times 10^{-4}$) in the central Labrador Sea, which is expected as this isopycnal outcrops in the winter. However, uLSW variance at downstream locales—Flemish Cap, the Grand Banks, and Cape Hatteras—are an order of magnitude larger ($\sim 20 \times 10^{-4}$) than the variance in the Labrador Sea (Figure 3a). An analysis of the local variance in the reanalysis product GloSea5 yields similar results, though GloSea5 has a broader region of strong variance from Flemish Cap to Cape Cod and no local maxima near Cape Hatteras (Figure S8 in Supporting Information S1). The local maxima in variance from the Flemish Cap to the Grand Banks is consistent with previous studies that describe this region as having leaky DWBC "hot spots" (e.g., Bower et al., 2011; Solodoch et al., 2020). This strong variance is generally attributed to mixing mechanisms, such as interactions with the nearby North Atlantic Current, which is known to meander and reach great depths (Rhein et al., 2019; Schott et al., 2006); leakage due to bathymetry curvature that leads to inertial separation (Solodoch et al., 2020); and submesoscale coherent vortices (Bower et al., 2013). We expect this strong local variance to be problematic for tracking advected anomalies downstream. Indeed, the uLSW max R^2 decreases rapidly from the Labrador Sea exit to the Flemish Cap and oscillates around 0.3 thereafter (Figure 3c).

The salinity variance on the dLSW isopycnal surface is everywhere less than that on the uLSW isopycnal. The dLSW salinity variance is maximum ($\sim 4 \times 10^{-4}$) in the central Labrador Sea and north of the Flemish Cap (Figure 3b). The analysis of the local variance in the reanalysis product GloSea5 yields similar results, yet with the difference that GloSea5 does not exhibit the variance maximum north of the Flemish Cap (Figure S8 in Supporting Information S1). Because of this relatively weak variance field, our expectation is that source water anomalies will more likely retain their source water signature as they move downstream on this isopycnal. Indeed, the dLSW max R^2 values are moderate to high along the DWBC. However, we note a small drop in the max R^2 and an increase in the local variance at the Flemish Cap and Grand Banks, suggesting a minor influence of mixing in this region.

3.3. Sensitivity of Results to Isopycnal Choice

To test the robustness of our results, we repeat the analyses from Sections 3.1 and 3.2 for a broader suite of isopycnals. To start, we have computed the salinity squared correlations with upstream anomaly (R^2) as a function

21699291, 2024, 12, Downloaded from https://agupubs.onlinelibrary.wiley.com/doi/10.1029/2024JC021241 by Georgia Institute Of Technology, Wiley Online Library on [07/01/2025]. See the Terms and Conditions (https://onlinelibrary.wiley.com/terms-and-conditions) on Wiley Online Library for rules of use; OA articles are governed by the applicable Creative Commons License

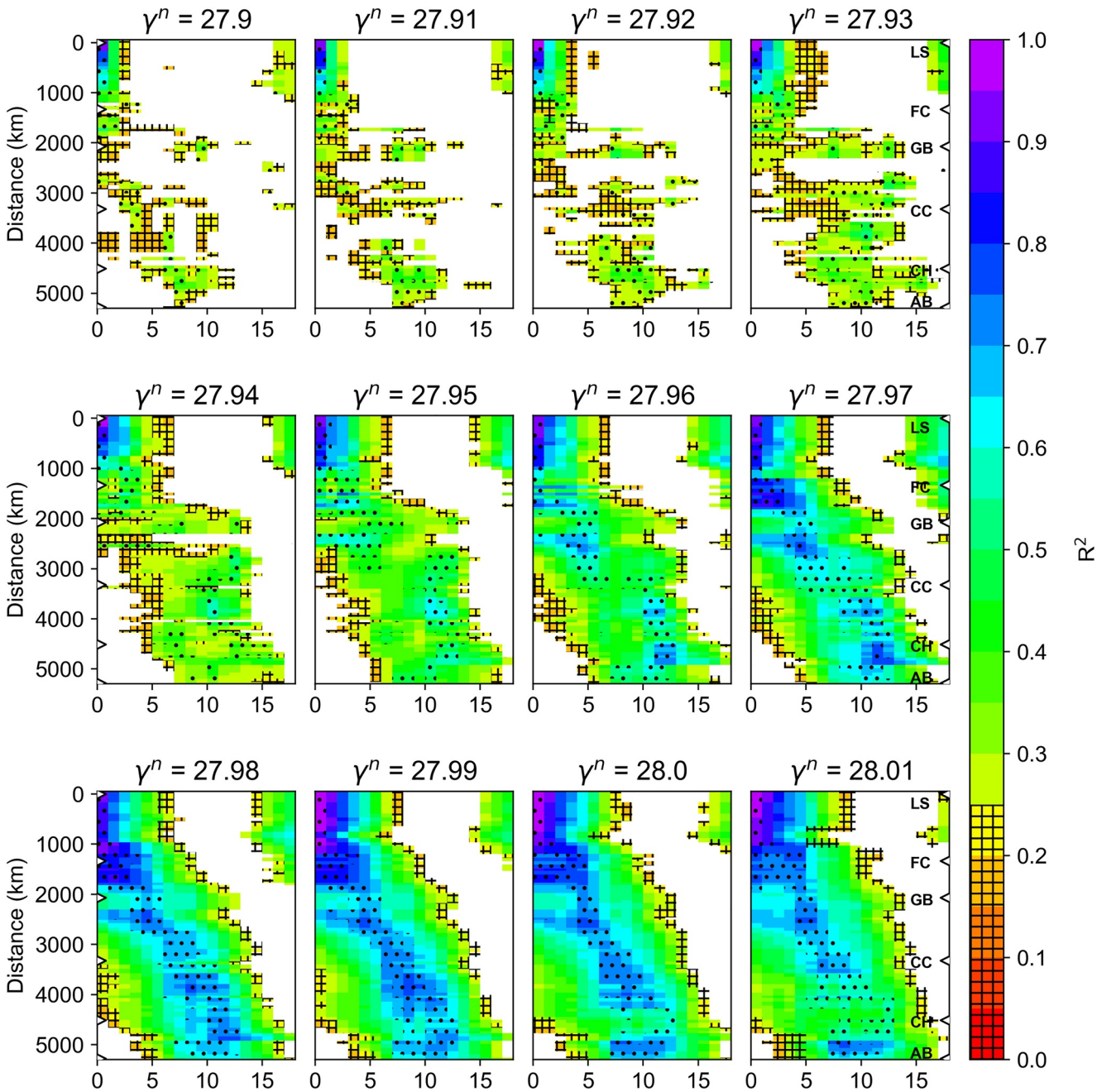

Figure 4. Salinity squared correlations with upstream anomalies (R^2) on various isopycnals between 27.9 and 28.01 along the Deep Western Boundary Current as a function of lag and distance from the Labrador Sea exit, where the Pearson correlation coefficient (R) is significant with a confidence interval of 99%. The dots indicates where R^2 is within 0.05 of its maximum over lags from 0 to 18 years; hatches indicate where $R^2 \leq 0.25$. For all panels, triangles indicate the Labrador Sea exit (LS); Flemish Cap (FC); Grand Banks (GB); Cape Cod (CC); Cape Hatteras (CH); and Abaco (AB).

of lag at each point along the DWBC with the Labrador Sea exit for all isopycnals between 27.90 and 28.01 with intervals of 0.01 kg/m^3 (Figure 4). For isopycnals 27.90 to 27.94, the lags are patchy and R^2 values are low, indicating weak if any downstream anomaly propagates. A signature of coherent propagation becomes visible at isopycnals 27.95 to 27.96. Although there is still discontinuity in the lag, the lag field is not as patchy as for the lighter isopycnals, and the R^2 values are stronger, though still moderate. Propagation becomes evident on isopycnals 27.97 to 28.01, as evidenced by the continuum in the lags and moderate to high R^2 values at all locations.

21699291, 2024, 12, Downloaded from https://agupubs.onlinelibrary.wiley.com/doi/10.1029/2024JC021241 by Georgia Institute Of Technology, Wiley Online Library on [07/01/2025]. See the Terms and Conditions (https://onlinelibrary.wiley.com/terms-and-conditions) on Wiley Online Library for rules of use; OA articles are governed by the applicable Creative Commons License

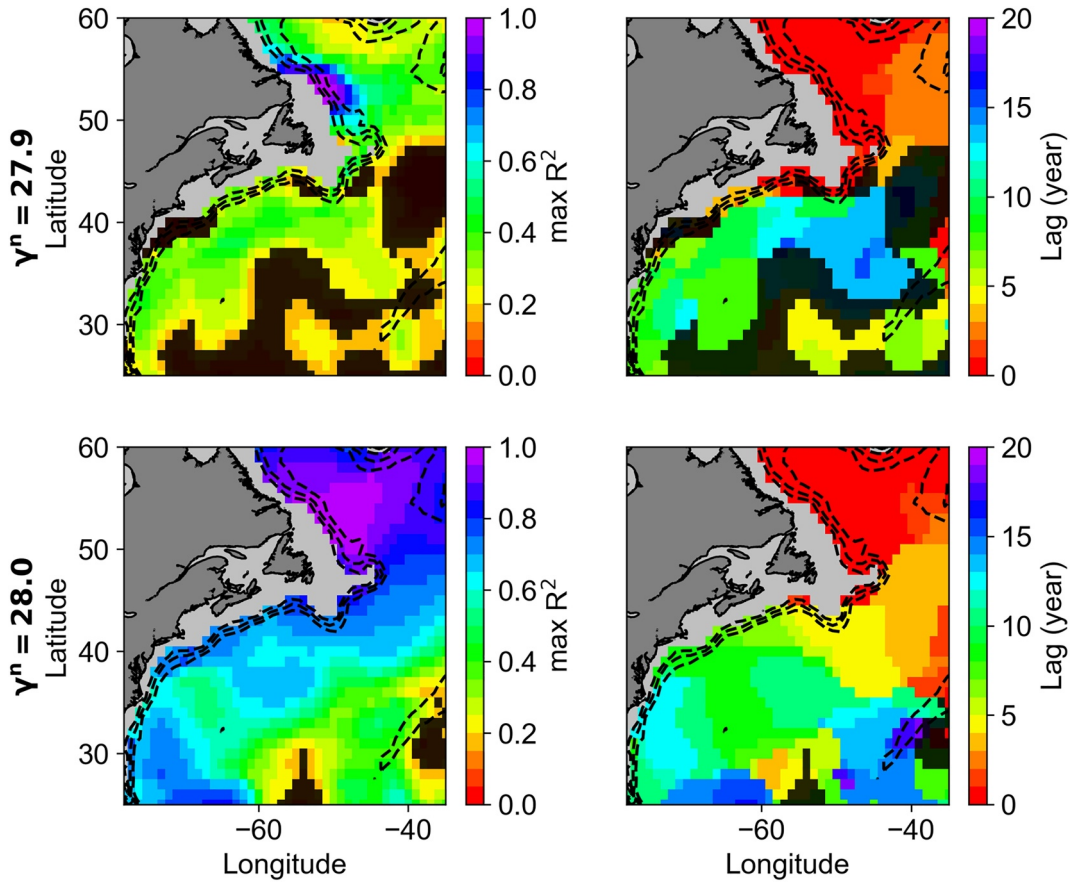

Figure 5. Left panels: Salinity maximum squared correlations with anomalies at the Labrador Sea exit (max R^2) on isopycnals 27.9 (uLSW) and 28.0 (dLSW) computed from the correlation at every grid point between the local salinity time series at the same at the Labrador Sea exit. Right panels: Lag corresponding to the max R^2 in the left panels. For all panels, areas where the Pearson correlation coefficient (R) is nonsignificant with a confidence interval of 99% have been masked. Dashed contours indicate the 1,000, 2,000, and 3,000 m isobaths from General Bathymetric Chart of the Ocean coarsened to 1°.

Furthermore, we have computed the salinity local variance as a function of distance with the Labrador Sea exit for all isopycnals between 27.90 and 28.01, with intervals of 0.01 kg/m^3, and its ratio of local to source variance (Figure S9 in Supporting Information S1). We observe that the local variance is punctuated by hotspots along the DWBC, particularly for isopycnals lighter than 27.95, which is the isopycnal range over which anomalies are not coherently propagated downstream. The magnitude of these hotspots is reduced on densities denser than 27.95, where the ratio of local to source variance downstream of the Flemish Cap is less than 1, that is, the local variance along the DWBC pathway is smaller than the source variance for dense isopycnals, consistent with the isopycnals range found for coherent anomaly propagation.

3.4. Broader Spatial Context

We now investigate the broader spatial context of subpolar to subtropical propagation by computing the max R^2 at all points and their associated lags for the uLSW and dLSW isopycnals over a wide swath of the western North Atlantic (Figure 5). As a reminder, R^2 results from the lagged correlation between the local time series at each grid with the time series at the exit of the Labrador Sea and represents what we term the advected variability.

For uLSW, only the area in the vicinity of the Labrador Sea exit shows a strong correlation between the local salinity time series and that at the Labrador Sea exit, with R^2 values > 0.5 in this area. The rest of the subpolar gyre, as well as the subtropical region offshore of the American coast, exhibits only moderate to low correlations, with R^2 values no greater than 0.5. The lags are small in the subpolar gyre and large in the subtropical gyre, with a steep increase at the inter-gyre boundary. Furthermore, while the lag pattern is quite uniform in the subpolar

21699291, 2024, 12, Downloaded from https://agupubs.onlinelibrary.wiley.com/doi/10.1029/2024JC021241 by Georgia Institute Of Technology, Wiley Online Library on [07/01/2025]. See the Terms and Conditions (https://onlinelibrary.wiley.com/terms-and-conditions) on Wiley Online Library for rules of use; OA articles are governed by the applicable Creative Commons License

region, it is patchy in the subtropical gyre. The subpolar pattern of low to moderate R^2 and low lags can be explained by uLSW formation each winter in this locale (explaining the low R^2) and local recirculation (explaining the lags). In the subtropics, the combination of a patchy pattern of high lags with low R^2 indicates a lack of coherent propagation for uLSW anomalies, as was seen for DWBC propagation. However, we note low lags along the DWBC from the subpolar gyre to Cape Cod. Downstream of that locale correlations are not statistically significant in the DWBC, but are significant in the interior basin , suggesting the importance of interior pathways from Cape Cod to Cape Hatteras for uLSW.

For dLSW, the local salinity time series are well correlated with that at the Labrador Sea exit, with R^2 values >0.8, over most of the subpolar area. While the strongest R^2 values are found in the DWBC, a band with width of ∼20° offshore of the DWBC shows moderate to high correlations, with R^2 values greater than 0.5. Over that area, there is a gradual southward increase in the lags which, combined with the moderate to high R^2 values, indicates coherent propagation for dLSW along interior pathways. The one exception to this pattern is the local minima for R^2 offshore of Cape Hatteras, which is consistent with the R^2 values along the DWBC discussed in Section 3.1. This spatial pattern reenforces past observational and modeling studies (Bower et al., 2009; Lozier et al., 2022; Petit et al., 2023) that have detailed the importance of interior pathways west of the Mid-Atlantic Ridge for the intrusion of NADW into the subtropics. To this point, the dLSW max R^2 pattern in Figure 5 is remarkably similar to the probability distribution map for modeled Lagrangian particles released in Northeast Atlantic Deep Water in the Irminger Sea (Figure 5 of Lozier et al., 2022).

Finally, the disparities between uLSW and dLSW in their maps of max R^2 and associated lag patterns across the North Atlantic basin are similar to what was previously found for the DWBC. That is, there is little evidence for coherent propagation of uLSW to the subtropical gyre, while there is strong evidence for coherent propagation for dLSW.

4. Summary

We use the EN4 data set to investigate the extent to which there is coherent propagation of property anomalies along the DWBC for upper and deep LSW from 1970 to 2020. We also use this data set to assess local property variance so that we can interpret the signatures of property propagation in the context of local mixing.

We find distinct differences in the extent to which properties propagate downstream in the DWBC as a function of isopycnals (Figures 2 and 4). On isopycnals that carry uLSW, there is little discernible downstream propagation of Labrador Sea anomalies past the Flemish Cap. Not only are there low R^2 on these isopycnals, but the lag from the Labrador Sea exit does not monotonically increase downstream, as would be expected if advection of anomalies dominated the local property field. Instead, the lags past the Flemish Cap are patchy with little discernible pattern. In contrast, there is strong evidence of coherent downstream anomaly propagation on isopycnals that carry dLSW. For these isopycnals, there is high to moderate R^2, and the lags uniformly increase along the DWBC. Taken together, these metrics indicate the coherent advection of property anomalies for dLSW.

Our analysis of the local property variability also reveals distinct differences between the isopycnals that carry uLSW and those that carry dLSW. On the shallower isopycnals the variance field is punctuated by known hotspots along the western boundary, associated with bathymetric features (Figure 3a). The local property variance at these hotspots is larger than the property variance in the Labrador Sea interior. In contrast, for the deeper isopycnals, the local variance along the DWBC is generally weaker than in the Labrador Sea interior (Figure 3b). In the competition between locally generated variability and advected variability, these results show that local variability is likely to dominate along the DWBC for the uLSW, while the advected variability is likely to dominate for the dLSW. Indeed, a direct comparison between local variability and advected variability shows this to be the case (Figures 3c and 3d). uLSW anomalies advected downstream quickly lose memory of their upstream anomaly in the face of local mixing. The dLSW property anomalies, however, retain their memory as their pathway along the DWBC is largely devoid of strong local mixing.

Furthermore, our investigation of the R^2 and their lags over a range of isopycnals shows a clear transition from uLSW to dLSW propagation characteristics, with the divide occurring at ∼27.95 (Figure 4). These propagation differences along the DWBC are also reflected in the broader subtropical North Atlantic (Figure 5). We find low R^2 and patchy lags for uLSW, indicating a lack of coherent propagation. In contrast, we find moderate to high R^2 and a gradual increase in the lags southward for dLSW on a 20°-wide continuous band offshore the DWBC. This

21699291, 2024, 12, Downloaded from https://agupubs.onlinelibrary.wiley.com/doi/10.1029/2024JC021241 by Georgia Institute Of Technology, Wiley Online Library on [07/01/2025]. See the Terms and Conditions (https://onlinelibrary.wiley.com/terms-and-conditions) on Wiley Online Library for rules of use; OA articles are governed by the applicable Creative Commons License

21699291, 2024, 12, Downloaded from https://agupubs.onlinelibrary.wiley.com/doi/10.1029/2024JC021241 by Georgia Institute Of Technology, Wiley Online Library on [07/01/2025]. See the Terms and Conditions (https://onlinelibrary.wiley.com/terms-and-conditions) on Wiley Online Library for rules of use; OA articles are governed by the applicable Creative Commons License

difference suggests that property variability and coherent propagation along interior pathways (Bower et al., 2009; Lozier et al., 2022; Petit et al., 2023) is also highly differentiated by density.

We conclude that property anomalies propagate to the subtropical gyre for the dLSW but there is no signature of coherent and persistent propagation for uLSW over 1970 to 2020 in the EN4 hydrographic data set. These results are consistent with Zou et al. (2019), who found these same differences for UNADW and LNADW, but for transport anomalies. The lack of meridional coherence in uLSW downstream of Flemish Cap and the increase in dLSW advection time at Flemish Cap (Figure 2) is also consistent with previous Lagrangian studies that observed LSW escapes from the DWBC in the vicinity of Flemish Cap for RAFOS floats launched at 700 and 1,500 m (Bower et al., 2009). Thus, our results reconcile the known propagation of LSW anomalies along the DWBC and the known entrainment and detrainment along that boundary.

As discussed in the Introduction, a wide range of LSW advective times has been reported in previous studies and a recent review has added insight into the probable cause for that range (Le Bras, 2023). For dLSW, the correlation coefficients we find here are significant for a wide range of lags (Figure 2). This wide range is consistent with the long-tail distribution seen in previous studies (e.g., Chomiak et al., 2022) and encompasses the advective time scales from previous studies focused on a particular observational window. For uLSW, we suggest that past reported correlations likely result from a focus on a large source water anomaly that can survive strong downstream mixing.

This distinction brings us to an important difference between our study and the recent Chomiak et al. (2023) study. Although our results are consistent with the reduced coherence of the convective signal for the shallow $LSW_{2000–2003}$ convective event ($\gamma^n = 27.90$) compared to the deep-reaching $LSW_{1987–1994}$ convective event ($\gamma^n = 27.99$), we argue that the difference noted between the two events is probably due to the isopycnal choice, not the strength of the anomaly. Though we did not investigate individual propagation events, anomaly strength influences the ratio between source and local variability, which ultimately determines the trackability of anomalies. Specifically, our analysis suggests that uLSW ($\gamma^n = 27.90$) experiences too much downstream mixing to preserve its anomalies. From our study, we conclude that there are different *memories* of the initial anomaly based on a competition between the strength of the initial anomaly and the local downstream variance. Since deeper isopycnals have smaller local variance along the DWBC we posit that: (a) An anomaly on a shallow isopycnal surface will likely not have a downstream signature; and (b) an anomaly on a dense isopycnal surface will likely be tracked downstream, especially if it has a strong initial signature.

In order to extend the spatial and temporal context of DWBC property propagation, we have relied on EN4. The use of this database, however, precludes our ability to extend our analysis to deeper isopycnals since EN4 observations are sparse below 2,000 m (Figure S1 in Supporting Information S1). An investigation of property propagation for overflow pathways will need to rely on observational data sets that capture water column properties in the deep ocean.

As the ocean property field continues to evolve in response to climate change, the fate of carbon and oxygen anomalies from the subpolar to the subtropical ocean is of increasing interest. As such, though our study has focused on salinity anomalies (and temperature anomalies by virtue of our isopycnal analysis), our results have relevance for the interpretation of downstream signatures of carbon and oxygen. Additionally, a follow-on observational study focused on the propagation of deep-water density anomalies along the western side of the North Atlantic basin would yield insight into the downstream coherence of AMOC and could possibly explain why Zou et al. (2019) found coherent propagation of transport anomalies for LNADW.

Data Availability Statement

All data sets and software used in the main text are referenced and available online. EN.4.2.2.analyses.g10 data were obtained from https://www.metoffice.gov.uk/hadobs/en4/ and are © British Crown Copyright, Met Office, 2022, provided under a Non-Commercial Government License http://www.nationalarchives.gov.uk/doc/non-commercial-government-licence/version/2/, last access 31 Oct. 2022. Please read Good et al. (2013) https://doi.org/10.1002/2013JC009067 for details of how the data set was constructed. GEBCO_2022 Grid (https://doi.org/10.5285/e0f0bb80-ab44-2739-e053-6c86abc0289c) is made freely available by the GEBCO Compilation Group (https://www.gebco.net/). OSNAP data (https://doi.org/10.35090/gatech/70342) were collected and made

freely available by the OSNAP (Overturning in the Subpolar North Atlantic Program) project and all the national programs that contribute to it (www.o-snap.org). We use the PreTEOS-10 software compute neutral density surfaces. The software is available at https://www.teos-10.org/preteos10_software/neutral_density.html and is described in Jackett and McDougall (1997); https://doi.org/10.1175/1520-0485(1997)027<0237:ANDVFT>2.0.CO;2.

Acknowledgments
This work was supported by the National Science Foundation Physical Oceanography Program (OCE-1948335). Any opinions, findings, and conclusions or recommendations expressed in this material are those of the author(s) and do not necessarily reflect the views of the National Science Foundation. The authors wish to thank Trevor McDougall and Paul Barker for providing valuable instructions in the use of PreTEOS-10 software (available at https://www.teos-10.org/preteos10_software/neutral_density.html) used to compute the neutral density surfaces. EN4.2.2.analyses.g10 data were obtained from www.metoffice.gov.uk/hadobs. The authors are grateful to Isabella Le Bras for providing Line W data sets in a convenient format and for helpful discussions. Finally, we wish to thank the two reviewers for their helpful comments.

References

Bilo, T. C., & Johns, W. (2019). Interior pathways of Labrador Sea water in the North Atlantic from the Argo perspective. *Geophysical Research Letters*, *46*(6), 3340–3348. https://doi.org/10.1029/2018GL081439

Blockley, E., Martin, M. J., McLaren, A. J., Ryan, A. G., Waters, J., Lea, D. J., et al. (2014). Recent development of the Met Office operational ocean forecasting system: An overview and assessment of the new Global FOAM forecasts. *Geoscientific Model Development*, *7*(6), 2613–2638. https://doi.org/10.5194/gmd-7-2613-2014

Bower, A., Lozier, S., & Gary, S. (2011). Export of Labrador Sea water from the subpolar North Atlantic: A Lagrangian perspective. *Deep Sea Research Part II: Topical Studies in Oceanography*, *58*(17–18), 1798–1818. https://doi.org/10.1016/j.dsr2.2010.10.060

Bower, A. S., Hendry, R. M., Amrhein, D. E., & Lilly, J. M. (2013). Direct observations of formation and propagation of subpolar eddies into the Subtropical North Atlantic. *Deep Sea Research Part II: Topical Studies in Oceanography*, *85*, 15–41. https://doi.org/10.1016/j.dsr2.2012.07.029

Bower, A. S., & Hunt, H. D. (2000). Lagrangian observations of the deep western boundary current in the North Atlantic Ocean: Part II: The Gulf stream–deep western boundary current crossover. *Journal of Physical Oceanography*, *30*(5), 784–804. https://doi.org/10.1175/1520-0485(2000)030<0784:LOOTDW>2.0.CO;2

Bower, A. S., Lozier, M. S., Gary, S. F., & Böning, C. W. (2009). Interior pathways of the North Atlantic meridional overturning circulation. *Nature*, *459*(7244), 243–247. https://doi.org/10.1038/nature07979

Brown, P. J., McDonagh, E. L., Sanders, R., Watson, A. J., Wanninkhof, R., King, B. A., et al. (2021). Circulation-driven variability of Atlantic anthropogenic carbon transports and uptake. *Nature Geoscience*, *14*(8), 571–577. https://doi.org/10.1038/s41561-021-00774-5

Chomiak, L., Volkov, D., & Schmid, C. (2023). The interior spreading story of Labrador Sea Water. *Frontiers in Marine Science*, *10*, 1270463. https://doi.org/10.3389/fmars.2023.1270463

Chomiak, L. N., Yashayaev, I., Volkov, D. L., Schmid, C., & Hooper, J. A. (2022). Inferring advective timescales and overturning pathways of the deep Western Boundary Current in the North Atlantic through Labrador Sea Water advection. *Journal of Geophysical Research: Oceans*, *127*(12), e2022JC018892. https://doi.org/10.1029/2022JC018892

Curry, R. G., McCartney, M. S., & Joyce, T. M. (1998). Oceanic transport of subpolar climate signals to mid-depth subtropical waters. *Nature*, *391*(6667), 575–577. https://doi.org/10.1038/35356

Doney, S. C., & Jenkins, W. J. (1994). Ventilation of the deep western boundary current and abyssal western North Atlantic: Estimates from tritium and 3 He distributions. *Journal of Physical Oceanography*, *24*(3), 638–659. https://doi.org/10.1175/1520-0485(1994)024<0638:VOTDWB>2.0.CO;2

Fine, R. A., Rhein, M., & Andrié, C. (2002). Using a CFC effective age to estimate propagation and storage of climate anomalies in the deep western North Atlantic Ocean. *Geophysical Research Letters*, *29*(24). 80-1. https://doi.org/10.1029/2002GL015618

Fu, Y., Lozier, M. S., Biló, T. C., Bower, A. S., Cunningham, S. A., Cyr, F., et al. (2023). Seasonality of the meridional overturning circulation in the subpolar North Atlantic. *Communications Earth & Environment*, *4*(1), 181. https://doi.org/10.1038/s43247-023-00848-9

GEBCO Compilation Group. (2022). GEBCO_2022 grid. https://doi.org/10.5285/e0f0bb80-ab44-2739-e053-6c86abc0289c

Good, S. A., Martin, M. J., & Rayner, N. A. (2013). EN4: Quality controlled ocean temperature and salinity profiles and monthly objective analyses with uncertainty estimates. *Journal of Geophysical Research: Oceans*, *118*(12), 6704–6716. https://doi.org/10.1002/2013JC009067

Gouretski, V., & Reseghetti, F. (2010). On depth and temperature biases in bathythermograph data: Development of a new correction scheme based on analysis of a global ocean database. *Deep Sea Research Part I: Oceanographic Research Papers*, *57*(6), 812–833. https://doi.org/10.1016/j.dsr.2010.03.011

Jackett, D. R., & McDougall, T. J. (1997). A neutral density variable for the world's oceans. *Journal of Physical Oceanography*, *27*(2), 237–263. https://doi.org/10.1175/1520-0485(1997)027<0237:ANDVFT>2.0.CO;2

Koelling, J., Atamanchuk, D., Karstensen, J., Handmann, P., & Wallace, D. W. R. (2022). Oxygen export to the deep ocean following Labrador Sea Water formation. *Biogeosciences*, *19*(2), 437–454. https://doi.org/10.5194/bg-19-437-2022

Le Bras, I. A., Yashayaev, I., & Toole, J. M. (2017). Tracking Labrador Sea water property signals along the deep western boundary current. *Journal of Geophysical Research: Oceans*, *122*(7), 5348–5366. https://doi.org/10.1002/2017JC012921

Le Bras, I. A.-A. (2023). Labrador Sea water spreading and the Atlantic meridional overturning circulation. *Philosophical Transactions of the Royal Society A*, *381*(2262), 20220189. https://doi.org/10.1098/rsta.2022.0189

Lozier, M. S., Bacon, S., Bower, A. S., Cunningham, S. A., Femke de Jong, M., de Steur, L., et al. (2017). Overturning in the Subpolar North Atlantic program: A new international ocean observing system. *Bulletin of the American Meteorological Society*, *98*(4), 737–752. https://doi.org/10.1175/BAMS-D-16-0057.1

Lozier, M. S., Bower, A. S., Furey, H. H., Drouin, K. L., Xu, X., & Zou, S. (2022). Overflow water pathways in the North Atlantic. *Progress in Oceanography*, *208*, 102874. https://doi.org/10.1016/j.pocean.2022.102874

Lozier, M. S., Roussenov, V., Reed, M. S. C., & Williams, R. G. (2010). Opposing decadal changes for the North Atlantic meridional overturning circulation. *Nature Geoscience*, *3*(10), 728–734. https://doi.org/10.1038/ngeo947

MacLachlan, C., Arribas, A., Peterson, K. A., Maidens, A., Fereday, D., Scaife, A. A., et al. (2015). Global seasonal forecast system version 5 (GloSea5): A high-resolution seasonal forecast system. *Quarterly Journal of the Royal Meteorological Society*, *141*(689), 1072–1084. https://doi.org/10.1002/qj.2396

Met Office Hadley Centre observations datasets. (2022). Retrieved from https://www.metoffice.gov.uk/hadobs/en4/index.html

Moat, B. I., Frajka-Williams, E., Smeed, D. A., Rayner, D., Johns, W. E., Baringer, M. O., et al. (2022). *Atlantic meridional overturning circulation observed by the RAPID-MOCHA-WBTS (RAPID-Meridional overturning circulation and heatflux array-western boundary time series) array at 26N from 2004 to 2020 (v2020.2)*. British Oceanographic Data Centre - Natural Environment Research Council, UK. https://doi.org/10.5285/e91b10af-6f0a-7fa7-e053-6c86abc05a09

Molinari, R. L., Fine, R. A., Wilson, W. D., Curry, R. G., Abell, J., & McCartney, M. S. (1998). The arrival of recently formed Labrador Sea water in the deep western boundary current at 26.5 N. *Geophysical Research Letters*, *25*(13), 2249–2252. https://doi.org/10.1029/98GL01853

21699291, 2024, 12, Downloaded from https://agupubs.onlinelibrary.wiley.com/doi/10.1029/2024JC021241 by Georgia Institute Of Technology, Wiley Online Library on [07/01/2025]. See the Terms and Conditions (https://onlinelibrary.wiley.com/terms-and-conditions) on Wiley Online Library for rules of use; OA articles are governed by the applicable Creative Commons License

Petit, T., Lozier, M. S., Rühs, S., Handmann, P., & Biastoch, A. (2023). Propagation and transformation of Upper North Atlantic Deep Water from the subpolar gyre to 26.5 N. *Journal of Geophysical Research: Oceans*, *128*(8), e2023JC019726. https://doi.org/10.1029/2023JC019726

Rhein, M., Mertens, C., & Roessler, A. (2019). Observed transport decline at 47 N, western Atlantic. *Journal of Geophysical Research: Oceans*, *124*(7), 4875–4890. https://doi.org/10.1029/2019JC014993

Schott, F. A., Fischer, J., Dengler, M., & Zantopp, R. (2006). Variability of the deep western boundary current east of the Grand Banks. *Geophysical Research Letters*, *33*(21). https://doi.org/10.1029/2006GL026563

Schott, F. A., Zantopp, R., Stramma, L., Dengler, M., Fischer, J., & Wibaux, M. (2004). Circulation and deep-water export at the western exit of the subpolar North Atlantic. *Journal of Physical Oceanography*, *34*(4), 817–843. https://doi.org/10.1175/1520-0485(2004)034<0817:cadeat>2.0.co;2

Smethie, W. M., Jr. (1993). Tracing the thermohaline circulation in the western North Atlantic using chlorofluorocarbons. *Progress in Oceanography*, *31*(1), 51–99. https://doi.org/10.1016/0079-6611(93)90023-7

Solodoch, A., McWilliams, J. C., Stewart, A. L., Gula, J., & Renault, L. (2020). Why does the deep western boundary current "leak" around flemish cap? *Journal of Physical Oceanography*, *50*(7), 1989–2016. https://doi.org/10.1175/JPO-D-19-0247.1

Solodoch, A., Stewart, A. L., & McWilliams, J. C. (2016). Baroclinic instability of axially symmetric flow over sloping bathymetry. *Journal of Fluid Mechanics*, *799*, 265–296. https://doi.org/10.1017/jfm.2016.376

Spall, M. A. (1996a). Dynamics of the Gulf Stream/deep western boundary current crossover. Part I: Entrainment and recirculation. *Journal of Physical Oceanography*, *26*(10), 2152–2168. https://doi.org/10.1175/1520-0485(1996)026<2152:DOTGSW>2.0.CO;2

Spall, M. A. (1996b). Dynamics of the Gulf Stream/deep western boundary current crossover. Part II: Low-frequency internal oscillations. *Journal of Physical Oceanography*, *26*(10), 2169–2182. https://doi.org/10.1175/1520-0485(1996)026<2169:DOTGSW>2.0.CO;2

Stramma, L., & Rhein, M. (2001). Variability in the deep western boundary current in the equatorial Atlantic at 44 W. *Geophysical Research Letters*, *28*(8), 1623–1626. https://doi.org/10.1029/2000GL011777

Toole, J., Curry, R., Joyce, T., McCartney, M., & Peña-Molino, B. (2011). Transport of the North Atlantic deep western boundary current about 39 N, 70 W: 2004–2008. *Deep Sea Research Part II: Topical Studies in Oceanography*, *58*(17–18), 1768–1780. https://doi.org/10.1016/j.dsr2.2010.10.058

van Sebille, E., Baringer, M. O., Johns, W. E., Meinen, C. S., Beal, L. M., de Jong, M. F., & van Aken, H. M. (2011). Propagation pathways of classical Labrador Sea water from its source region to 26 N. *Journal of Geophysical Research*, *116*(C12), C12027. https://doi.org/10.1029/2011JC007171

Waugh, D. W., & Hall, T. M. (2005). Propagation of tracer signals in boundary currents. *Journal of Physical Oceanography*, *35*(9), 1538–1552. https://doi.org/10.1175/JPO2779.1

Zou, S., Lozier, M. S., & Buckley, M. (2019). How is meridional coherence maintained in the lower limb of the Atlantic meridional overturning circulation? *Geophysical Research Letters*, *46*(1), 244–252. https://doi.org/10.1029/2018GL080958

21699291, 2024, 12, Downloaded from https://agupubs.onlinelibrary.wiley.com/doi/10.1029/2024JC021241 by Georgia Institute Of Technology, Wiley Online Library on [07/01/2025]. See the Terms and Conditions (https://onlinelibrary.wiley.com/terms-and-conditions) on Wiley Online Library for rules of use; OA articles are governed by the applicable Creative Commons License